

**Molecular Clouds and Star Formation: A  
Multiwavelength Study of Perseus, Serpens, and  
Ophiuchus**

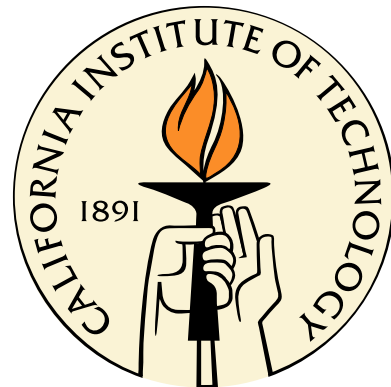
Thesis by

Melissa L. Enoch

In Partial Fulfillment of the Requirements

for the Degree of

Doctor of Philosophy



California Institute of Technology

Pasadena, California

2008

(Defended June 8, 2007)

© 2008

Melissa L. Enoch

All Rights Reserved

# Acknowledgements

Having at last reached the end of this long and often daunting expedition, I find myself at somewhat of a loss as to how to adequately express my appreciation for all of the help, support, and guidance that has gotten me here. But if graduate school has taught me anything, it is to just put pen to paper (or fingers to keyboard) and hope for the best.

This thesis could not have been completed without the help and collaboration of many people. Over the years that I have worked with her, my advisor, Anneila Sargent, has always forced me to focus on the larger picture, for which I am eternally grateful. I know that the lessons she has taught me will continue to improve my work, my papers, and my presentations for many years.

Working on the earliest phases of star formation at Caltech can be a lonely venture at times, but I have been lucky enough to have a number of collaborators at other institutions who have taken interest in my work, particularly Neal Evans at the University of Texas and Jason Glenn at the University of Colorado. I can safely say that this thesis would not exist without our many useful discussions, telecons, emails, and sometimes even battles. Being involved with the “Cores to Disks” *Spitzer* Legacy project has been an invaluable resource, not only for the wealth of data but for the collaborations it has generated. The c2d group meetings have sparked some of my most productive work, and the discussions, questions, and suggestions of many c2d members helped to keep me excited about my research.

I am indebted to the many members of the Bolocam instrument team, in particular Sunil Golwala, Jack Sayers, and Glenn Laurent, who patiently answered questions and helped me to develop the iterative mapping routine used for reduction of the Bolocam

data presented here. The analysis of the Ophiuchus Bolocam data would not have been possible without the help of Kaisa Young, who completed the data reduction and initial analysis. I am grateful to John Carpenter, who never kicked me out of his office when I insisted on pestering him with stupid questions. Thank you to my committee members, Nick Scoville, Re'em Sari, John Carpenter, and Sunil Golwala, for useful comments and questions that helped to focus my research, and for not giving me too much grief about the length of this thesis.

On a more personal note, my fellow classmates, Laura, Cathy, Stuart, Milan, Margaret, and Elina, have been my lifeline here at Caltech, keeping me afloat through our first year and sharing the many ups and downs of the following five. To everyone else who helped to make grad school bearable in the tough times and fun in the not so tough; thanks to Dave for the pizza and movies, Dan for the gossip, the girls for the cosmos, and the boys for the forties.

My family is a consistent and unwavering source of support, always providing a much needed sanctuary for escape and regeneration. Knowing that they would have supported me even if I had run away to cooking school somehow made it easier to carry on. Although she probably doesn't realize it, my sister Paige is a constant inspiration. My love and appreciation to all of you. Finally, thanks to Monica, who will always be my oldest friend, for stubbornly believing that I could do anything, even graduate. And to Tom, for keeping me (mostly) sane.

# Abstract

In this thesis I utilize large-scale millimeter and mid- to far-infrared surveys to address a number of outstanding questions regarding the formation of low mass stars in molecular clouds. Continuum  $\lambda = 1.1$  mm maps completed with Bolocam at a resolution of  $31''$  cover the largest areas observed to date at millimeter or submillimeter wavelengths in three molecular clouds:  $7.5 \text{ deg}^2$  in Perseus ( $140 \text{ pc}^2$  at the adopted distance of  $d = 250 \text{ pc}$ ),  $10.8 \text{ deg}^2$  ( $50 \text{ pc}^2$  at  $d = 125 \text{ pc}$ ) in Ophiuchus, and  $1.5 \text{ deg}^2$  ( $30 \text{ pc}^2$  at  $d = 125 \text{ pc}$ ) in Serpens. These surveys are sensitive to dense substructures with mean density  $n \gtrsim 2 - 3 \times 10^4 \text{ cm}^{-3}$ . A total of 122 cores are detected in Perseus, 44 in Ophiuchus, and 35 in Serpens above mass detection limits of  $0.1 - 0.2 M_\odot$ . Combining with *Spitzer* mid- and far-infrared maps from the c2d Legacy program provides wavelength coverage from  $\lambda = 1.25 - 1100 \mu\text{m}$ , and enables the assembly of an unbiased, complete sample of the youngest star forming objects in three environments. This sample includes 108 prestellar cores, 43 Class 0 sources and 94 Class I sources.

The approximately equal number of starless cores and embedded protostars in each cloud implies a starless core lifetime of  $2 - 4 \times 10^5 \text{ yr}$ , only a few free-fall timescales. This timescale, considerably shorter than the timescale predicted by the classic scenario of magnetic field support in which core evolution is moderated by ambipolar diffusion, suggests that turbulence is the dominant process controlling the formation and evolution of dense cores. However, dense cores in all three clouds are found only at high cloud column densities, where  $A_V \gtrsim 7 \text{ mag}$ , and the fraction of cloud mass in these cores is less than 10%, indicating that magnetic fields must play some role as well. Measured angular deconvolved sizes of the majority of starless

cores are consistent with radial density profiles substantially flatter than  $\rho \propto r^{-2}$ , or with Bonnor-Ebert spheres. The prestellar core mass distribution (CMD) has a slope of  $\alpha = -2.5 \pm 0.2$  for  $M > 0.8 M_{\odot}$ , remarkably similar to recent measurements of the slope of the stellar initial mass function:  $\alpha = -2.3$  to  $-2.8$ . While this result does not rule out the importance of feedback or competitive accretion, it provides support for the hypothesis that stellar masses are determined during the core formation process.

The lifetime of the Class 0 phase is estimated to be  $1 - 2 \times 10^5$  yr in Perseus and Serpens, or approximately half that of the Class I phase, arguing against a very rapid early accretion phase. In Ophiuchus the fraction of Class 0 sources is much smaller, consistent with previous measurements of a short ( $\sim 10^4$  yr) Class 0 phase in that cloud. A large population of low luminosity Class I sources that cannot be explained by constant or monotonically decreasing accretion rates is observed in each cloud. This result strongly suggest that accretion during the Class I phase is episodic, with sources spending approximately 25% of the Class I lifetime in a quiescent state.

Finally, I investigate the environmental dependence of star formation by comparing the dense core populations of the three clouds. Cores are found at considerably higher cloud column densities in Ophiuchus than in Perseus or Serpens; more than 75% of cores occur at visual extinctions of  $A_V \gtrsim 8$  mag in Perseus,  $A_V \gtrsim 15$  mag in Serpens, and  $A_V \gtrsim 20 - 23$  mag in Ophiuchus. Cloud CMDs are well characterized by power-law fits ( $dN/dM \propto M^{\alpha}$ ) above their empirically derived 50% completeness limits, resulting in slopes of  $\alpha = -2.1 \pm 0.1$  in Perseus,  $\alpha = -2.1 \pm 0.3$  in Ophiuchus, and  $\alpha = -1.6 \pm 0.2$  in Serpens. Measured slopes for Perseus and Ophiuchus broadly agree with turbulent fragmentation, but the relative shapes of the observed cloud CMDs are inconsistent with detailed simulations of the dependence of CMD shape on Mach number.

# Contents

<b>1</b>	<b>Introduction</b>	<b>1</b>
1.1	A Star is Born . . . . .	1
1.1.1	Working Model for Isolated Star Formation . . . . .	2
1.1.2	Outstanding Questions . . . . .	5
1.1.3	Global Processes: Magnetic Fields versus Turbulence . . . . .	6
1.1.4	Core Initial Conditions . . . . .	10
1.1.5	Early Protostellar Evolution . . . . .	16
1.1.6	Effects of Environment . . . . .	19
1.2	Observations . . . . .	22
1.2.1	Millimeter Surveys . . . . .	22
1.2.1.1	Prestellar Cores . . . . .	23
1.2.1.2	Masses . . . . .	24
1.2.2	Infrared Surveys . . . . .	26
1.2.2.1	“Cores to Disks” Legacy Program . . . . .	27
1.3	Thesis Goals and Outline . . . . .	28
	Bibliography . . . . .	31
<b>2</b>	<b>Bolocam Survey for 1.1 mm Dust Continuum Emission in the Perseus Molecular Cloud</b>	<b>37</b>
	Abstract . . . . .	37
2.1	Introduction . . . . .	38
2.2	Observations . . . . .	42
2.3	Data Reduction . . . . .	45

2.3.1	Pointing . . . . .	45
2.3.2	Removal of Sky Noise . . . . .	46
2.3.3	Mapping and Calibration . . . . .	48
2.3.4	Iterative Mapping . . . . .	50
2.3.4.1	Method . . . . .	50
2.3.4.2	Performance . . . . .	51
2.4	Results . . . . .	56
2.4.1	Source Identification . . . . .	56
2.4.2	Comparison to Molecular and $A_V$ Maps . . . . .	61
2.4.3	Source Statistics . . . . .	67
2.5	Discussion . . . . .	83
2.5.1	Completeness and the Mass versus Size Distribution . . . . .	83
2.5.2	The 1.1 mm Mass Function . . . . .	87
2.5.3	Clustering . . . . .	92
2.5.4	An Extinction Threshold for 1.1 mm Cores . . . . .	95
2.5.5	Comparison to c2d Observations: B1 Ridge . . . . .	97
2.6	Summary . . . . .	99
	Acknowledgments . . . . .	100
	Bibliography . . . . .	102
<b>3</b>	<b>Bolocam Survey for 1.1 mm Dust Continuum Emission in the Ophiuchus Molecular Cloud</b>	<b>107</b>
	Abstract . . . . .	107
3.1	Introduction . . . . .	108
3.2	Observations . . . . .	109
3.3	Data Reduction . . . . .	111
3.3.1	Pointing and Flux Calibration . . . . .	111
3.3.2	Iterative Mapping . . . . .	112
3.3.3	Source Identification . . . . .	112
3.4	Results . . . . .	113

3.4.1	General Cloud Morphology . . . . .	113
3.4.2	Source Properties . . . . .	119
3.4.2.1	Positions and Photometry . . . . .	119
3.4.2.2	Sizes and Shapes . . . . .	126
3.4.2.3	Masses, Densities, and Extinctions . . . . .	128
3.5	Discussion . . . . .	130
3.5.1	Completeness . . . . .	130
3.5.2	The Core Mass Distribution . . . . .	132
3.5.3	Clustering . . . . .	135
3.5.4	Extinction threshold . . . . .	138
3.6	Summary . . . . .	142
	Acknowledgments . . . . .	143
	Bibliography . . . . .	144
<b>4</b>	<b>Bolocam Survey for 1.1 mm Dust Continuum Emission in the Serpens Molecular Cloud</b>	<b>147</b>
	Abstract . . . . .	147
4.1	Introduction . . . . .	147
4.2	Observations and Data Reduction . . . . .	149
4.2.1	Observations . . . . .	149
4.2.2	Pointing and Flux Calibration . . . . .	151
4.2.3	Cleaning and Mapping . . . . .	151
4.2.4	Source Identification . . . . .	152
4.3	Results . . . . .	155
4.3.1	Comparison to Visual Extinction . . . . .	157
4.3.2	Source Properties . . . . .	159
4.3.2.1	Positions and Photometry . . . . .	159
4.3.2.2	Sizes and Shapes . . . . .	164
4.3.2.3	Masses, Densities, and Extinctions . . . . .	165
4.4	Summary . . . . .	167

Acknowledgments . . . . .	168
Bibliography . . . . .	169
<b>5 Comparing Star Formation on Large Scales in the c2d Legacy Clouds: Bolocam Surveys of Serpens, Perseus, and Ophiuchus 171</b>	
Abstract . . . . .	171
5.1 Introduction . . . . .	172
5.2 Three-Cloud Sample . . . . .	174
5.3 What is a Core? . . . . .	174
5.4 Distance Effects . . . . .	178
5.5 Discussion . . . . .	181
5.5.1 Physical Implications of Source Sizes and Shapes . . . . .	181
5.5.2 Densities and the Mass versus Size Distribution . . . . .	185
5.5.3 Fragmentation and the Core Mass Distribution . . . . .	188
5.5.4 Clustering . . . . .	192
5.5.5 Relationship to Cloud Column Density . . . . .	196
5.5.6 Efficiency of Forming Cores . . . . .	198
5.6 Summary . . . . .	201
Acknowledgments . . . . .	204
Bibliography . . . . .	205
<b>6 Prestellar Cores and Deeply Embedded Protostars with Spitzer and Bolocam: Properties of the Youngest Objects in Perseus, Serpens, and Ophiuchus 207</b>	
Abstract . . . . .	207
6.1 Introduction . . . . .	208
6.2 Combining Bolocam and Spitzer c2d Data . . . . .	212
6.3 Identifying Cold Protostars . . . . .	219
6.3.1 Association with a 1.1 mm Core . . . . .	222
6.3.2 Separating Starless and Protostellar Cores . . . . .	224
6.4 Comparing the Starless and Protostellar 1.1 mm Core Populations . .	226

6.4.1	Sizes and Shapes . . . . .	227
6.4.2	Core Densities . . . . .	230
6.4.3	The Mass versus Size Distribution . . . . .	234
6.4.4	Core Mass Distributions . . . . .	237
6.4.5	Relationship to Cloud Column Density . . . . .	239
6.4.6	Clustering . . . . .	241
6.5	The Prestellar Core Mass Distribution . . . . .	243
6.6	Properties of Cold Protostars . . . . .	249
6.6.1	Bolometric Luminosity and Temperature . . . . .	249
6.6.2	Envelope Mass . . . . .	250
6.6.3	Completeness . . . . .	250
6.6.4	Individual Sources . . . . .	255
6.6.4.1	IRAS 03292+3039 . . . . .	255
6.6.4.2	Pers-Bolo 102 . . . . .	257
6.6.4.3	Serp-Bolo 33 and Other Class II Objects . . . . .	259
6.7	Comparison of Classification Methods . . . . .	262
6.7.1	Alternative Classifications . . . . .	269
6.8	Protostellar Evolution . . . . .	271
6.9	Lifetimes . . . . .	280
6.9.1	Timescale of the Class 0 Phase . . . . .	280
6.9.2	Timescale of the Prestellar Phase . . . . .	283
6.10	Conclusions . . . . .	285
	Acknowledgments . . . . .	287
6.11	Appendix: Calculating the bolometric luminosity and temperature . .	289
	Bibliography . . . . .	294
<b>7</b>	<b>Summary and Future work</b>	<b>299</b>
7.1	Summary . . . . .	299
7.2	The Future . . . . .	305
7.2.1	Main Accretion Phase Lifetime . . . . .	306

7.2.2	Tracing Structure Near the Protostar . . . . .	306
7.2.3	Timescale for Disk Formation and the Disk Mass Fraction . .	308
	Bibliography . . . . .	311

# List of Figures

1.1	Standard schematic picture of how an isolated low mass star forms . . . . .	3
1.2	Correlation between measured core lifetime and mean density . . . . .	9
1.3	Core mass distribution for extinction-identified cores in the Pipe Nebula	13
1.4	Correlation between source angular size and density profile index . . . .	15
1.5	Simple protostellar evolution models for an exponentially decreasing accretion rate . . . . .	18
1.6	Core mass distributions resulting from turbulent fragmentation simulations . . . . .	21
2.1	Observational coverage of Bolocam and IRAC maps in Perseus, overlaid on an integrated intensity $^{13}\text{CO}$ map . . . . .	44
2.2	Iterative mapping performance: NGC 1333 . . . . .	52
2.3	Iterative mapping performance: Fractional lost peak flux density . . . .	54
2.4	Iterative mapping performance: Fractional lost integrated flux density	55
2.5	Bolocam 1.1 mm map of the Perseus molecular cloud . . . . .	57
2.6	Bolocam map of Perseus, with high source density regions magnified and sources identified . . . . .	59
2.7	Examples of new millimeter detections in Perseus . . . . .	60
2.8	Comparison of 1.1 mm emission and visual extinction in Perseus . . . .	63
2.9	Comparison of 1.1 mm emission and $^{13}\text{CO}$ integrated intensity in Perseus	64
2.10	$A_V$ calculated from the 1.1 mm emission in Perseus . . . . .	65
2.11	Distribution of source peak and total flux densities in Perseus . . . .	80
2.12	Distribution of source minor and major axis FWHM sizes in Perseus . .	81
2.13	Distribution of source axis ratios in Perseus . . . . .	82

2.14	Total mass versus FWHM size for sources in Perseus, with empirically derived completeness curves . . . . .	84
2.15	Total mass versus size at the $3\sigma$ contour for sources in Perseus . . . . .	86
2.16	Differential mass distribution for sources in Perseus . . . . .	88
2.17	Characterization of the dependence on dust temperature of the core mass distribution . . . . .	90
2.18	Two-point correlation function for sources in Perseus . . . . .	94
2.19	Probability of finding a 1.1 mm core as a function of $A_V$ for sources in Perseus . . . . .	96
2.20	Comparison of Bolocam and Spitzer maps in the B1 Ridge . . . . .	98
3.1	Observational coverage of Bolocam and IRAC maps in Ophiuchus, overlaid on a visual extinction map . . . . .	110
3.2	Bolocam 1.1 mm map of the Ophiuchus molecular cloud . . . . .	114
3.3	Map of the $1\sigma$ rms noise in Ophiuchus . . . . .	115
3.4	Bolocam map of Ophiuchus, with high source density regions magnified and sources identified . . . . .	116
3.5	MIPS three-color image of the eastern streamer in Ophiuchus, with 1.1 mm contours . . . . .	118
3.6	Comparison of 1.1 mm emission and visual extinction in Ophiuchus . .	120
3.7	Distribution of source peak and total flux densities in Ophiuchus . . .	127
3.8	Distribution of source minor and major axis FWHM sizes in Ophiuchus	128
3.9	Total mass versus FWHM size for sources in Ophiuchus, with empirically derived completeness curves . . . . .	131
3.10	Differential mass distribution for sources in Ophiuchus . . . . .	133
3.11	Two-point correlation function for sources in Ophiuchus . . . . .	137
3.12	Probability of finding a 1.1 mm core as a function of $A_V$ for sources in Ophiuchus . . . . .	139
3.13	Flux density, size, and mass versus $A_V$ for sources in Ophiuchus . . . .	140

4.1	Observational coverage of Bolocam, IRAC, and MIPS maps in Serpens, overlaid on a visual extinction map . . . . .	150
4.2	Bolocam 1.1 mm map of the Serpens molecular cloud . . . . .	153
4.3	Map of the $1\sigma$ rms noise in Serpens . . . . .	154
4.4	Bolocam map of Serpens, with high source density regions magnified and sources identified . . . . .	156
4.5	Comparison of 1.1 mm emission and visual extinction in Serpens . . .	158
4.6	Distribution of source peak and total flux densities in Serpens . . . .	163
4.7	Distribution of source minor and major axis FWHM sizes in Serpens .	164
4.8	Differential mass distribution for sources in Serpens . . . . .	166
5.1	Completeness as a function of linear deconvolved source size in Serpens, Perseus, and Ophiuchus . . . . .	176
5.2	Comparison of source properties for the original and degraded-resolution Ophiuchus samples: sizes, shapes, masses, and densities . . . . .	179
5.3	Ratio of angular deconvolved size to beam size for the original and degraded-resolution Ophiuchus samples . . . . .	180
5.4	Comparison of linear and angular deconvolved source sizes in Serpens, Perseus, and Ophiuchus . . . . .	182
5.5	Comparison of source axis ratios in Serpens, Perseus, and Ophiuchus .	184
5.6	Comparison of core mean densities measured at the half-maximum and $4\sigma$ contours in Serpens, Perseus, and Ophiuchus . . . . .	186
5.7	Total mass versus angular deconvolved size for sources in Serpens, Perseus, and Ophiuchus . . . . .	187
5.8	Comparison of the core mass distributions for Serpens, Perseus, and Ophiuchus . . . . .	189
5.9	Comparison of the two-point correlation function for Serpens, Perseus, and Ophiuchus . . . . .	194
5.10	Cumulative fraction of 1.1 mm cores as a function of cloud $A_V$ for Serpens, Perseus, and Ophiuchus . . . . .	197

6.1	three-color Spitzer images (8.0, 24, 160 $\mu$ m) of selected starless cores in Perseus, Serpens, and Ophiuchus . . . . .	214
6.2	three-color Spitzer images (8.0, 24, 70 $\mu$ m) and SEDs of selected protostellar cores in Perseus . . . . .	216
6.3	three-color Spitzer images and SEDs of selected protostellar cores in Serpens . . . . .	217
6.4	three-color Spitzer images and SEDs of selected protostellar cores in Ophiuchus . . . . .	218
6.5	Selection criteria for the cold protostar samples . . . . .	220
6.6	Protostellar selection criteria applied to galaxy candidates . . . . .	221
6.7	Distribution of the distance from cold protostar candidates in Perseus to the nearest core position, compared to a random distribution . . . . .	223
6.8	Angular deconvolved sizes of starless and protostellar cores in Perseus, Serpens, and Ophiuchus . . . . .	228
6.9	Axis ratios of starless and protostellar cores . . . . .	229
6.10	Peak column densities of protostellar and starless cores . . . . .	232
6.11	Mean densities of protostellar and starless cores . . . . .	233
6.12	Mass versus size for starless and protostellar cores in Perseus . . . . .	235
6.13	Mass versus size for protostellar and starless cores in Serpens and Ophiuchus . . . . .	236
6.14	Mass distributions of protostellar and starless cores in Perseus, Serpens, and Ophiuchus . . . . .	238
6.15	Cumulative fraction of starless and protostellar cores as a function of cloud $A_V$ . . . . .	240
6.16	Two-point correlation function for protostellar and starless cores . . . . .	242
6.17	Combined prestellar core mass distribution . . . . .	245
6.18	Combined protostellar core mass distribution . . . . .	247
6.19	three-color <i>Spitzer</i> image (3.6, 24, 70 $\mu$ m) of IRAS 03292+3039 (Pers-Cold 2) . . . . .	257
6.20	three-color <i>Spitzer</i> image (8, 24, 70 $\mu$ m) of Pers-Bolo 102 . . . . .	258

6.21	three-color <i>Spitzer</i> image of Serp-Cold 33 . . . . .	260
6.22	Bolometric temperature versus spectral index $\alpha_{IR}$ for cold protostar candidates in Perseus, Serpens, and Ophiuchus . . . . .	263
6.23	Distribution of $T_{bol}$ as a function of distance to the nearest 1.1 mm core for cold protostar candidates in Perseus, Serpens, and Ophiuchus . . .	264
6.24	Distribution of $\alpha_{IR}$ as a function of distance to the nearest 1.1 mm core	265
6.25	Average spectra for Class 0, Class I, and Class II . . . . .	266
6.26	Results of fitting Ophiuchus source SEDs to average Class 0 and Class I spectra . . . . .	268
6.27	Average spectra for designated $T_{bol}$ bins: “early Class 0,” “late Class 0,” etc. . . . .	270
6.28	Results of fitting cold protostar candidate SEDs to template average spectra . . . . .	272
6.29	$L_{bol}$ versus $T_{bol}$ for cold protostars, compared to evolutionary models .	274
6.30	Average spectra for “non-envelope Class I,” and low- $L_{bol}$ sources . . . .	277
6.31	$M_{env}$ versus $T_{bol}$ for cold protostars, compared to evolutionary models .	279
6.32	Comparison of methods for calculating $T_{bol}$ . . . . .	290
6.33	Characterization of sampling errors for $T_{bol}$ and $L_{bol}$ . . . . .	291
6.34	Characterization of errors in $T_{bol}$ for missing 160 $\mu\text{m}$ fluxes . . . . .	292
7.1	Example of using IRS spectra to probe small-scale envelope structure .	307
7.2	Example of separating disk and envelope contributions in an embedded protostar . . . . .	309



# List of Tables

1.1	Millimeter and submillimeter bolometer arrays . . . . .	23
2.1	Identified sources in Perseus . . . . .	69
2.2	Photometry, masses, sizes, and morphology for sources in Perseus . . .	73
3.1	Identified sources in Ophiuchus . . . . .	121
3.2	Photometry, masses, sizes, and morphology for sources in Ophiuchus .	123
3.3	Cumulative mass as a function of extinction for sources in Ophiuchus	141
4.1	Identified sources in Serpens . . . . .	160
4.2	Photometry, masses, sizes, and morphology for sources in Serpens . .	161
5.1	Cumulative mass as a function of extinction for sources in Serpens, Perseus, and Ophiuchus . . . . .	199
6.1	Statistics of 1.1 mm cores in the three clouds . . . . .	226
6.2	Bolometric temperatures, luminosities, and envelope masses of cold protostars in Perseus . . . . .	251
6.3	Bolometric temperatures, luminosities, and envelope masses of cold protostars in Serpens . . . . .	253
6.4	Bolometric temperatures, luminosities, and envelope masses of cold protostars in Ophiuchus . . . . .	255
6.5	Class II sources detected at 1.1 mm in Perseus, Serpens, and Ophiuchus	260
6.6	Relative numbers of starless, Class 0, and Class I sources . . . . .	280